[Scanning Microscopy](https://digitalcommons.usu.edu/microscopy)

Volume 1 | Number 1 Article 2

12-18-1986

Morphological Characterization of Materials using Low Voltage Scanning Electron Microscopy (LVSEM)

Jesse Hefter
GTE Laboratories Incorporated

Follow this and additional works at: https://digitalcommons.usu.edu/microscopy

Part of the Life Sciences Commons

Recommended Citation

Hefter, Jesse (1986) "Morphological Characterization of Materials using Low Voltage Scanning Electron Microscopy (LVSEM)," *Scanning Microscopy*: Vol. 1 : No. 1 , Article 2.
Available at: https://digitalcommons.usu.edu/microscopy/vol1/iss1/2

This Article is brought to you for free and open access by the Western Dairy Center at DigitalCommons@USU. It has been accepted for inclusion in Scanning Microscopy by an authorized administrator of DigitalCommons@USU. For more information, please contact digitalcommons@usu.edu.

Scanning Microscopy, Vol. 1, No. 1, 1987 (Pages 13-21) 0981-7035/87$3.00+.00
Scanning Microscopy International, Chicago (AMF O'Hare), IL 60666 USA

MORPHOLOGICAL CHARACTERIZATION OF MATERIALS USING LOW VOLTAGE SCANNING ELECTRON MICROSCOPY (LVSEM)

Jesse Hefter

GTE Laboratories Incorporated
40 Sylvan Road
Waltham, MA 02254

(Received for publication September 13, 1986, and in revised form December 18, 1986)

Abstract

The use of lower energy (0.5 to 10 keV) electron beams in the scanning electron microscope (LVSEM) provides a number of advantages in the imaging of materials, including increased topographic contrast and reduced specimen charging. Application of LVSEM to materials analysis was difficult in the past due to a number of instrumental difficulties, including low gun brightness, the increased effect of chromatic aberration upon lower energy beams, and the increased sensitivity of such electron beams to stray fields. Improvements in design have led to commercial instruments which provide the microscopist with the capability to analyze materials in this low-energy regime. LVSEM has been applied to the analysis of a variety of specimens, all of which would have proven quite difficult or impossible by "classical" higher-energy (15-35 keV) SEM. Examples discussed include an ion-implanted cemented carbide, a surface-modified glassy carbon electrode, a semiconductor (III-V) layered structure, and a macroscopic polymer crystal.

Key words: Low Voltage Scanning Electron Microscopy, materials analysis, topographic contrast, secondary electron imaging, electron range, charge reduction, spatial resolution.

*** Address for correspondence:**

Jesse Hefter
GTE Laboratories Incorporated
40 Sylvan Rd.
Waltham, MA 02254
Phone No.: 617-466-2778

Introduction

The advent of commercial scanning electron microscopes (SEM) with excellent spatial resolution at low electron beam energies has led to a resurgence of interest in the use of low voltage SEM (LVSEM) for the imaging of a wide variety of materials. In large part, LVSEM has mainly seen application in the semiconductor field (Menzel and Kubalek, 1985; Hashimoto et al., 1982) and, to a lesser degree, in the imaging of biological materials (Dilly, 1980). In addition to the two areas of focus mentioned above, a third area of application is to general materials analysis. It is the intent of this paper to describe the use of LVSEM in the morphological characterization of a variety of materials and thereby to stimulate the interest of other workers in applying this technique to the solving of similar and other materials analysis problems.

Background

The use of probing electron beams having relatively high energies (25-40 keV) in the SEM has been a preferred mode of operation due to a number of important considerations. First, the use of high-energy primary electrons allows for maximizing the beam current for a given desired electron probe diameter. This permits optimum resolution and signal-to-noise ratio on conducting and coated specimens. Secondly, commercially available instruments did not allow the operator the convenience of easily adjusting the instrument for use at lower working energies (e.g., low gun brightness at low beam energies leading to decreased signal-to-noise ratio and the necessity of realignment of the optical column) (Volbert, 1984). Additional technical limitations which delayed the more widespread use of LVSEM (e.g., increased effects of chromatic aberration and sensitivity of lower energy electron beams to stray fields) are described in an excellent review by Pawley (1984).

The use of lower energy (1–10 keV) primary electron beams provides a number of important advantages. Firstly, the range of penetration of primary electrons into a solid specimen decreases as the energy of the entering primary electron is lowered. Thus, the production of secondary electrons (SE) is restricted to a smaller specimen volume. Among the SE produced are (a) those due to direct inelastic scattering (SE1 = Secondary Electron–Type I) and (b) those resulting from additional inelastic scattering (SE2 = Secondary Electron–Type II). The former electrons carry the surface-sensitive information since they derive from the immediate surface region of the electron probe impact point. The SE2 tend to mask the direct surface electron signal as they are generated by backscattered electrons which scatter up to the specimen surface and can be generated at some lateral distance from the electron impact point (Joy, 1985; The typological scheme for various kinds of SE is after Drescher et al., 1970.)

Secondly, charging of nonconductive or poorly conducting materials is reduced and in some cases eliminated (Goldstein et al., 1984a). This reduction of charging at LV occurs within a certain range of primary electron energies because a balance between the number of secondary and backscattered electrons exiting the sample and the number of primary electrons entering it may be achieved (Flinn and Salehi, 1981). An important practical result of the reduction of charging is that the necessity of coating insulating specimens is often eliminated.

An important consideration in the use of LVSEM is the spatial resolution obtainable. If the electron beam is sufficiently low in energy so as to make the electron range comparable to the SE escape range, then resolution as good as that attainable at higher beam energies may be obtained (provided that a finely focused electron beam can be maintained). A comprehensive discussion of spatial resolution in LVSEM based on the use of Monte Carlo simulation techniques has been presented by Joy (1985).

Experimental

The LVSEM imaging was carried out using the JSM-840II analytical scanning electron microscope (Japan Electron Optics Laboratory, Tokyo). This instrument provides an accelerating voltage range of 0.2–40 kV. A standard tungsten hairpin filament was used for all imaging work. A set of images were taken for each specimen at a variety of beam energies. For the purposes of this work, a small imaging probe was formed by using a 50 μm objective aperture and a probe current (measured by the use of a beam stop) in the range of 1–15 pA (usually 1–5 pA). Working distances in the range of 8–28 mm were used. Photomicrographs were taken onto Polaroid Type 52 Black/White film generally using an exposure time of 100 s (vertical scan time).

Sample A. The semiconductor sample consisted of two sections (a specular and a nonspecular region) of a Si wafer which had been coated by MOCVD-grown GaAs to a thickness of ≈ 1 μm. The specimens were mounted onto a brass stub using conductive silver paint.

Sample B. The carbide sample consisted of a WC-6% Co cemented carbide tool insert which had been implanted perpendicularly to the surface with nitrogen at a fluence of $2 \times 10^{17} N_2^+/cm^2$ and at an implantation energy of 120 keV. The corresponding implantation depth was 57 nm. Microhardness measurements were made with a LECO-M400LF tester at an indentation load of 10 g. The specimen was mounted in a spring-loaded specimen holder with no pretreatment.

Sample C. A glassy carbon electrode (0.3 cm diameter, Tokai, Japan) was first polished with 600-grit emery cloth and then with 0.3 μm Al_2O_3 suspended in water. The electrode was then electrochemically modified in 8M H_2SO_4 by a cyclic voltammetric method. The specimen was mounted vertically onto a brass specimen stub with conductive silver paint as the adhesive.

Sample D. The polymer sample consisted of chemically modified polydiacetylene (PDA) resulting from bromination of 1,6-di-N- carbazolyl-2,4-hexadiyne (DCH). The fibrous, rust-colored polymer sample was affixed to a specimen stub with double-sided adhesive tape. A change in the exposure time (50 s rather than the normal 100 s) was necessitated for photomicrography of the SE images (to reduce charging artifacts).

Results

A set of photomicrographs taken of three different areas in the specular region of the GaAs/Si specimen at 20, 10, and 4 keV beam energy (25,000x, normal beam incidence) are shown, respectively, in Figures 1a–1c. Photomicrographs of three areas in the nonspecular region taken at the same conditions as those for the specular region are presented in Figures 2a–2c. A comparison of two surface images, one of which was obtained at normal beam incidence and one at a specimen tilt of 25° (beam energy: 4 keV; 10,000x) is presented in Figures 3 and 4.

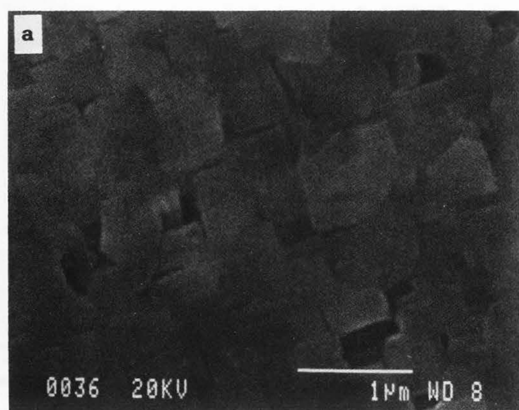

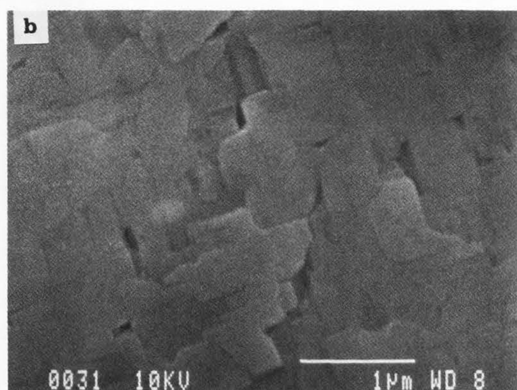

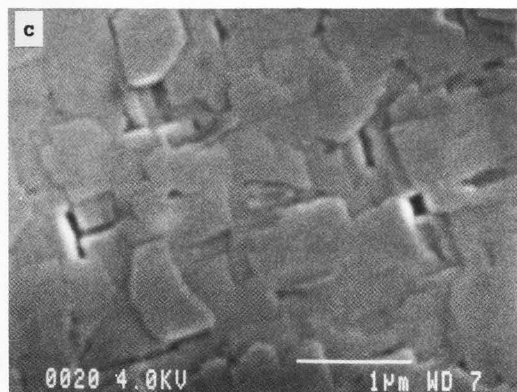

Fig. 1. SEM image of specular region on GaAs/Si wafer at:

(a) 20 keV, normal incidence;

(b) 10 keV, normal incidence;

(c) 4 keV, normal incidence.

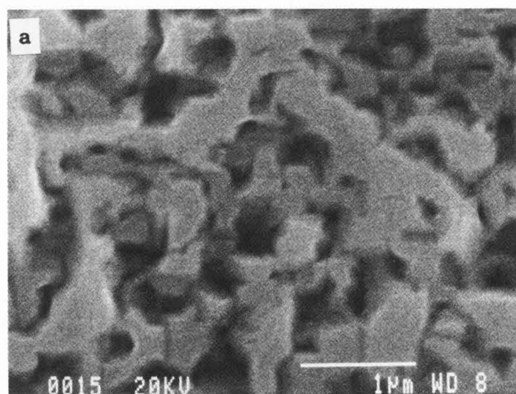

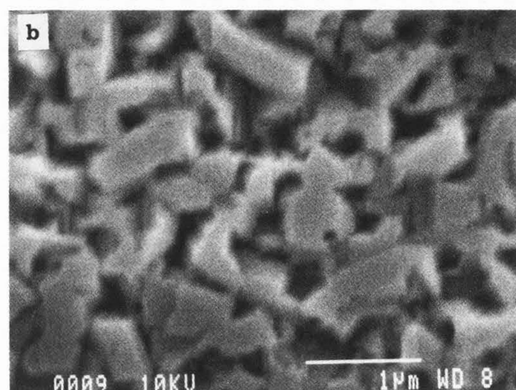

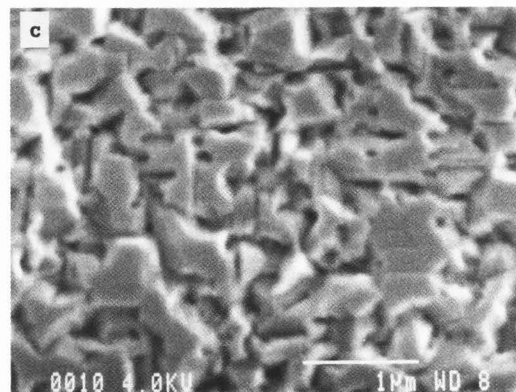

Fig. 2. SEM images of nonspecular region on GaAs/Si at:

(a) 20 keV, normal incidence;

(b) 10 keV, normal incidence;

(c) 4 keV, normal incidence.

Images of a low-load indentation in the surface of the ion-implanted cemented carbide taken at three beam energies (25, 15, and 5 keV; magnification: 8000x) are presented in Figures 5a-5c. A graphical representation of the approximate electron range data for the cemented carbide in the 1-20 keV range is shown in Figure 6. Photomicrographs of a feature located at the surface of the modified glassy carbon electrode taken at 23, 13, and 3 keV (10,000x) are displayed in Figures 7a-7c. Finally, imaging data for the PDA specimen

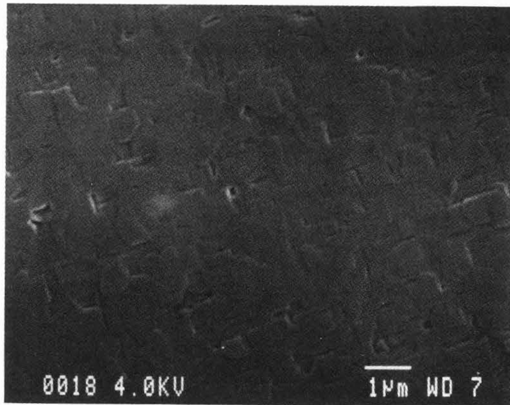

Fig. 3. LVSEM images of specular region on GaAs/Si at 4 keV, normal incidence.

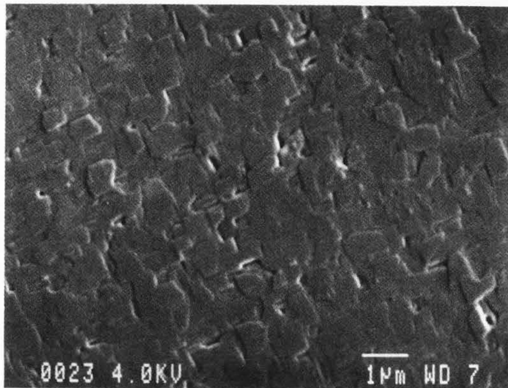

Fig. 4. LVSEM images of specular region on GaAs/Si at 4 keV, 25° specimen tilt.

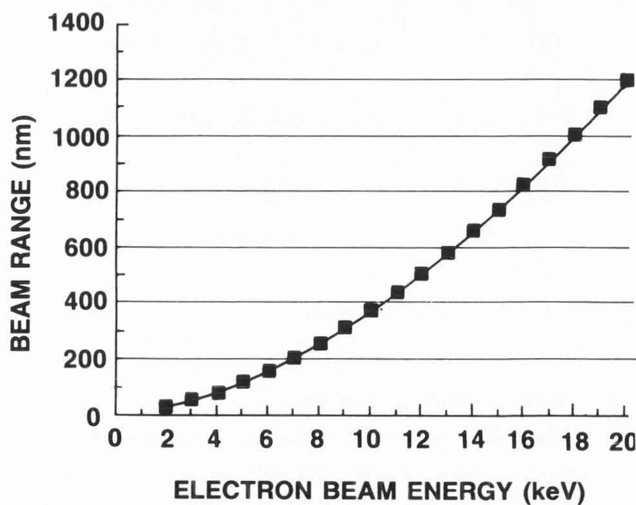

Fig. 6. Calculated electron beam penetration depth vs. electron beam energy for WC/6 wt%-Co.

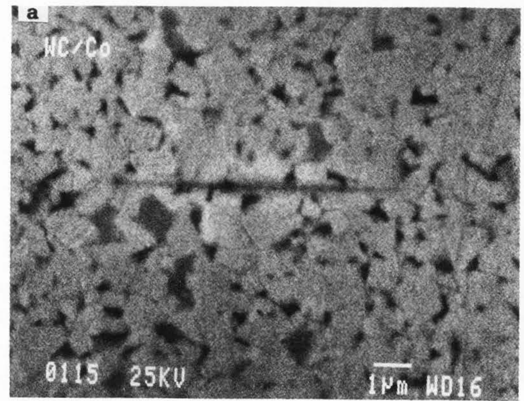

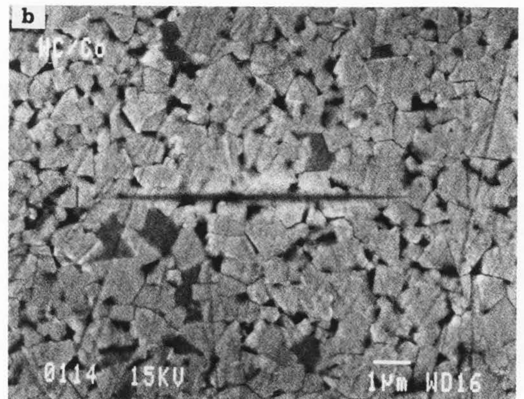

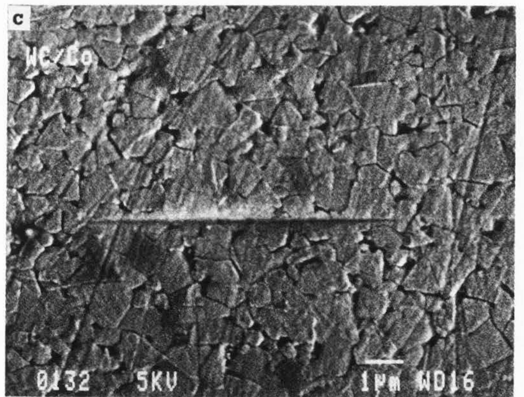

Fig. 5. SEM images of low-load indent in an ion-implanted cemented carbide at:

(a) 25 keV;

(b) 15 keV;

(c) 5 keV.

taken at 1 keV are given in Figure 8 (250x) and Figure 9 (500x).

Discussion

The range of an electron beam into a specimen

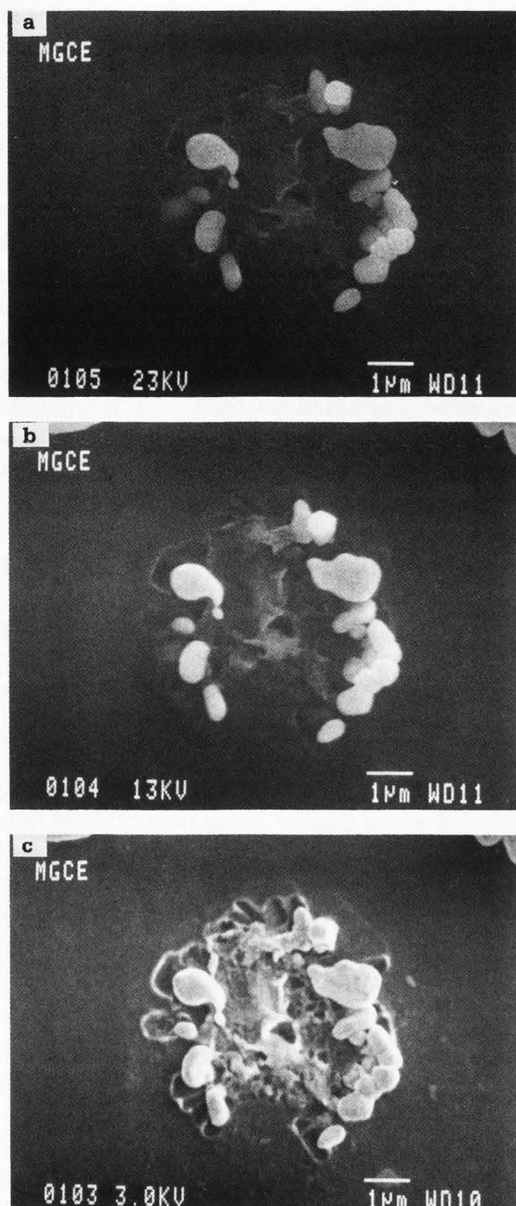

Fig. 7. SEM images of feature on modified glassy carbon electrode surface at:

(a) 23 keV;

(b) 13 keV;

(c) 3 keV.

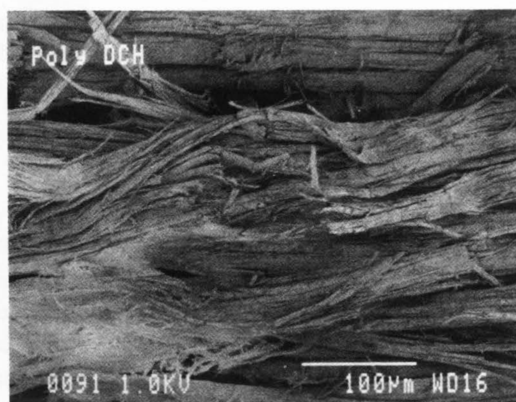

Fig. 8. LVSEM images of polydiacetylene specimen at normal beam incidence.

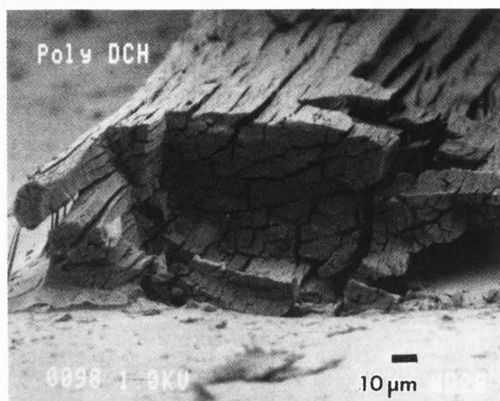

Figure 9. LVSEM images of polydiacetylene specimen at 79° specimen tilt.

decreases as the energy of the beam decreases. A number of models have been proposed which take into account energy loss of the electron (inelastic scattering) as a result of electronic collisions and directional deflections (elastic scattering) as a result of nuclear scattering. For obtaining a qualitative estimate of the electron range, the semi-empirical, modified diffusion model of Kanaya and Okayama (1972) was used. The maximum electron range (RKO) can be expressed as in Equation (1):

$$R_{KO} = 0.0276\ A\ E_o^{1.67}/(Z^{0.889}\varrho)\ \mu m \qquad (1)$$

where A is the atomic (or molecular) weight (g/mol), E_o is the beam energy (keV), Z is the atomic number (or average atomic number for a compound), and ϱ is the density (g/cm^3). Thus, for the cemented carbide specimen, values obtained for R_{KO} at 20, 10, and 5 keV are respectively 1.2, 0.37, and 0.12 μm. It is immediately appreciated that a reduction in beam energy by a factor of four (20 to 5) leads to an order of magnitude decrease in the maximum electron range for this sample. This result bears directly upon the imaging results discussed below for this specimen.

Gallium Arsenide/Silicon

The ability of LVSEM to provide image information from the near-surface of a specimen is shown here. Thus, in the case of a wafer having both specular and

nonspecular regions, it is important to determine what surface features give rise to the loss of specularity. For example, Figures 1a-1c show the difference in surface detail obtainable by imaging the specular surface over a range of beam energies. The surface detail (edge contrast and feature height information) is shown best in the LV image (Figure 1c). In contrast, the image shown in Figure 1a (taken at 20 keV) shows a somewhat flattened surface topography. This is expected since at the higher beam energy, the area over which the SE2 are emerging is larger than that at substantially lower incident beam energies (Joy, 1985). Thus, the SE1 signal is reduced in the overall detected electron signal count. The results at 10 keV, as expected, show feature contrast somewhat intermediate to that in the 20 and 4 keV images.

The physical height of these raised features was experimentally determined by cross-sectioning a specimen and observing the GaAs and its upper surface by transmission electron microscopy (TEM, Philips EM-400T, 120 keV). Heights on the order of $\approx$46 nm were found.

The results for the nonspecular region follow a trend similar to that shown for the specular region. Images obtained from employing a progression of decreasing beam energies (Figures 2a-2c) clearly indicate how additional surface features become evident as the beam energy is lowered. The image taken at 4 keV contains significantly more topographic information; surface details having vertical dimensions on the order of 50 nm can be seen. Further, a greater sense of the height variations at the surface can be readily apprehended. Cross-sectional TEM investigations of this region indicated height variations ranging from 30 to 230 nm.

It has been shown experimentally that the secondary electron yield (the number of electrons generated/incident primary electron) increases as the angle of specimen tilt increases (Goldstein et al., 1984b). Two reasons advanced for this effect are (1) that the number of SE generated (and detected) is related to the path length of the primary electron and that this path length increases as the angle of entry of the electron into the specimen decreases (from normal incidence), and (2) that the number of backscattered electrons generated also increases with specimen tilt and that these also produce more SE that are detected. However, whereas the angular distribution of backscattered electrons becomes asymmetric in the forward direction as the tilt angle increases, the angular distribution for the secondary electrons remains a cosine function (Goldstein et al., 1984a; Seiler, 1983). The variation in topographic information obtainable by tilting the specimen is shown for the specular region in Figures 3 and 4. It is clear that the surface detail obtainable at 25° is better than that obtained at normal incidence. Since the features of interest along the surface of the region are not very high ($\approx$46 nm), the electron range in GaAs even at 4 keV ($\approx$350 nm) is sufficient to render them difficult to image. The use of specimen inclination provides an additional contrast mechanism which leads to improved surface imaging. This is accomplished partly by decreasing the penetration depth to a moderate degree and also by accenting several types of topographic contrast such as "particle" or "micro-roughness" contrast (Peters, 1984).

Ion-Implanted Cemented Carbide

The use of LVSEM in the studies of microhardness and topography of ion-implanted cemented carbides has been described recently by Hefter et al. (1985). Ion implantation with high fluence ion beams is used to modify the surface of a variety of solid-state materials, including metals and ceramics (Burnett and Page, 1984). The types of ion implantation described here yield implanted zones having depths on the order of 200 nm. In order to carry out microhardness measurements on such a near-surface region, it is critical that only the upper modified surface be tested. This may be accomplished by employing low-load indentation techniques. The use of classical (higher beam energy) SEM imaging to observe the indents is made quite difficult since the electron range and associated high degree of lateral beam spreading leads to the obscuring of the surface detail and allows only an estimate of the indent length to be obtained (Figure 5a). In contrast, the endpoints of the indent are much more clearly observed at lower beam energies (cf. Figure 5c). The intermediate energy situation (Figure 5b) shows surface detail intermediate to that shown in the other two figures.

The approximate length of the indent found for this specimen is 8 μm (this length range is near the resolution limit of an optical microscope and therefore necessitates the use of SEM, especially for the precise measurement of the distance between the indent endpoints). It is known that the depth of the indent at its center is $\approx$1/25 of the indent length (from the geometry of the indenter tip). Thus, it is calculated that the deepest portion of the indent is 320 nm. A consideration of the effect of beam energy upon electron range is important at this juncture. A plot of the range versus beam energy is presented in Figure 6. It is seen that at energies greater than 9 keV, the electron range (and to a first approximation, the dimension of lateral beam spreading) is of sufficient magnitude to degrade the image of the indent even in its largest surface topographic feature regions. It is further evident that the required resolution of the indent endpoint (necessitating

an electron range ≈ lateral beam spreading of about 50 nm) will require the use of a beam energy ≈3 keV.

Glassy Carbon Electrode

The chemically modified glassy carbon electrode surface contains a number of interesting features resulting from chemical and electrochemical treatments. For correlating the effect of different chemistries and electrical treatments with the electrode surface morphology, it is necessary that clear images of the surface structures themselves are obtained. The image data of the structure shown in Figures 7a-7c indicate to what degree the surface detail may be imaged as the energy of the probing electron beam is reduced. A considerably greater amount of surface topographic information can be obtained from the photomicrograph taken at 3 keV as opposed to that gotten at a beam energy of 13 keV.

Macroscopic Polymer Crystal

The improvement of conjugated polymeric systems for both enhanced electronic and optical properties is an area of active research interest (Sandman and Cukor, 1984). The solid-state polymerization of single-crystal DCH to form a crystalline polymer has been described (Sandman et al., 1986a). Preliminary SEM imaging data taken at 15 keV beam energy of a brominated-poly-(DCH) have also been described (Sandman et al., 1986b). It was shown that the polymer maintained a fibrous structure not unlike that of the pristine polymer. In the prior work it was necessary to coat the polymer sample with an evaporated metal layer (Au/Pd, ≈15 nm) in order to prevent excessive charging.

The application of LVSEM allows the imaging of the material without the need of sample coating. In addition, the technique affords the potential of observing clear surface details which might otherwise be obscured due to the large penetration depth of the electron beam into the organic material at higher beam energies. The use of electron beam energies >5 keV for imaging the uncoated polymer sample led to immediate sample charging (as well as observable irradiation damage). This charging was dramatically reduced as the beam energy was lowered from 4 to 2 keV. The images shown in Figures 8 and 9 were obtained at a beam energy of 1 keV. The fibrous nature of the polymer is accented in Figure 8 (250x), where structures approximately 1 μm in size can be seen. The parallel nature of the polymer chain stacking is shown in Figure 9 (500x, 79° tilt). This topographic ("perspective") view provides significant insights as to the mode of polymer growth and general polymer chain orientation. No apparent specimen damage was noted during the acquisition of these image data.

Conclusion

It has been shown that the use of low voltage SEM provides the materials scientist with a powerful analytical tool useful in the characterization of a variety of materials. LVSEM imaging allows for the observation of uncoated specimens, allows for higher resolution surface imaging, and may allow for decreased irradiation damage. In this work, the use of LVSEM allowed the imaging of fine surface detail of a specular region on a GaAs/Si wafer and permitted acquisition of exceptionally clear images of low-load indentations in ion-implanted cemented carbides. In addition, the technique yielded important data as to the morphology both of surface deposits on a carbon electrode and of the fibrous nature of a highly ordered macroscopic polymer crystal.

Acknowledgements

The assistance of K. Ostreicher in obtaining the corroborative TEM data of the GaAs/Si specimen is gratefully acknowledged. The assistance of P. E. Norris, D. W. Oblas, M. L. Bowers, and D. J. Sandman in providing samples and useful discussions is also appreciated.

References

Burnett PJ, Page TF. (1984). Modifying the tribological properties of ceramics by ion-implantation. Br. Ceram. Proc. **34**, 65-76.

Dilly PN. (1980). Enhanced contrast of cilia using low accelerating voltage as an aid to low power survey and counting. Scanning **3**, 283-284.

Drescher H, Reimer L, Seidel H. (1970). Backscattering and secondary electron emission of 10-100 keV electrons and correlations to scanning electron microscopy. Z. Angew. Phys. **29**(6), 331-336.

Flinn EA, Salehi M. (1981). Accuracy of theoretical predictions concerning the location of the crossover points on the secondary electron emission yield curve. J. Appl. Phys. **52**(9), 5800-5802.

Goldstein JI, Newbury DE, Echlin P, Joy DC, Fiori C, Lifshin E. (1984a). Scanning Electron Microscopy and

X-Ray Microanalysis — A Text for Biologists, Material Scientists, and Geologists, Plenum, NY, 461-467.

Goldstein JI, Newbury DE, Echlin P, Joy DC, Fiori C, Lifshin E. (1984b). Scanning Electron Microscopy and X-Ray Microanalysis — A Text for Biologists, Material Scientists, and Geologists, Plenum, NY, 93-95.

Hashimoto N, Todokoro H, Fukahara S, Senoo K. (1982). Process characterization of MOS devices by scanning electron microscopy with 0.5-1 kV electrons. (Proc. 13th Conf. Solid State Devices, Tokyo, 1981); Jpn. J. Appl. Phys. Part 1; **21**, Suppl. 21-1, 199-203.

Hefter J, Oblas DW, Emma TA. (1985). Low-voltage SEM surface studies of microhardness and topography of ion-implanted cemented carbides., in: Proc. 43rd Ann. Meet. Electr. Microsc. Soc. Amer., G.W. Bailey (ed), San Francisco Press, 280-281.

Joy DC. (1985). Resolution in low voltage scanning electron microscopy. J. Microsc. **140** (3), 283-292.

Kanaya K, Okayama S. (1972). Penetration and energy-loss theory of electrons in solid targets. J. Phys. D: Appl. Phys. **5**, 43-58.

Menzel E, Kubalek E. (1985). Some recent developments in low voltage E-beam testing of ICs. J. Microsc. **140** (3), 331-349.

Pawley J. (1984). Low voltage scanning electron microscopy. J. Microsc. **136** (1), 45-68.

Peters K-R. (1984). Scanning Electron Microscopy: Contrast at High Magnification., in: Microbeam Analysis - 1984, AD Romig, JI Goldstein (eds.), San Francisco Press, 77-80.

Sandman DJ, Cukor P. (1984). Introduction to the symposium on order in polymeric materials. Mol. Cryst. Liq. Cryst. **105** (1), 1-10.

Sandman DJ, Elman BS, Hamill GP, Velazquez CS, Samuelson LA. (1986a). Solid state polymerization and the chemical reactivity of solid polydiacetylenes. Mol. Cryst. Liq. Cryst. **134,** 89-107.

Sandman DJ, Elman BS, Hamill GP, Hefter J, Velazquez CS. (1986b). The chemical modification of poly-1,6-Di-N-Carbazolyl-2,4-hexadiyne: diffraction, microscopy, and magnetism studies. Mol. Cryst. Liq. Cryst. **134,** 109-119.

Seiler H. (1983). Secondary electron emission in the scanning electron microscope. J. Appl. Phys. **54** (11), R1-R13, and references therein.

Volbert B. (1984). Low voltage scanning electron microscopy and its applications, Electron Opt. Rep. **31**, (1EM), 44-53.

Discussion with Reviewers

L. Reimer: There is no discussion in the paper of atomic number contrast in the interpretation of the micrographs. The backscattering coefficients at low energies show less differences [Reimer L, Tollkamp C (1980). Measuring the backscattering coefficient and secondary electron yield inside a scanning electron microscope. Scanning 3 (1), 35–39]. All comparisons of high and low energy micrographs confirm that the material contrast decreases with decreasing energies below 5 keV. Is there not some evidence for this in the micrographs in Figures 5a-5c?

Author: Yes, the micrographs do exhibit this effect.

H. Seiler: Interesting results with LVSEM should occur at the maximum of secondary electron emission (i.e., PE energies of some 100 eV). The SEM used in this study provides accelerating voltage range down to 200 eV. Why are images taken no lower than at PE energies of 3 and 4 keV shown?

C. Tollkamp-Schierjott: Most of the photographs are taken at 20, 10, and 4 keV. There is still a remarkable difference in surface information between 4 and 1 keV. Would it not have been more convenient to present the examples at even lower primary energy than 4 keV?

Author: It is probable that the use of beam energies lower than 3-4 keV can provide for additional insight into the surface morphology. One mitigating factor, however, was the magnification necessary to perform some of the imaging. At lower beam energies, although the electron range decreases, chromatic aberration effects can begin to play a more important role and make it difficult to obtain a final probe size comparable to that obtainable at higher energies. A limiting magnification of ≈20,000x at 1 keV is generally obtainable with the instrument used. Since higher magnifications than this value were desired, somewhat higher beam energies were used. Further, in general the imaging of these specimens was carried out at higher energies first, and then followed by slowly decreasing the beam energy and observing the resulting image (with calculated values of the expected electron range to act as a guide). In the 3-5 keV range, excellent quality micrographs were obtained. Below these values, good images can be obtained but were not necessary for the purposes of this work. Finally, in the case of the polymer crystal (Figures 8 and 9), the images are taken using a beam energy of 1 keV.

H. Seiler: Can you specify your vacuum conditions? Normally, the contamination rate is higher for low PE energies than for high PE energies.
Author: The specified vacuum for the instrument (in the specimen chamber) is in the 1–5 × 10^{-6} torr range.

H. Seiler: Is the degree of specimen damage in the low voltage regime comparable to that obtained at high PE energies and how would it pertain to the investigation of thin foils, thin films, and small particles on metallic bulk materials?
Author: Pawley (1984) has pointed out that a 1 keV electron beam at a 10^{-11} A beam current yields a beam power of 10^{-8} W. If this beam impinges upon an SEM specimen in a 1000 nm raster to an extent of only the upper 10 nm of the surface, then the calculated dose rate (assuming only half the energy to be absorbed) is on the order of 5 × 10^{5} J/g-s. This energy density is sufficiently high to cause ionizing radiation damage to SEM specimens. In the case of biological specimens, extensive physical damage will still occur at low PE energies, thus limiting spatial resolution. For thin foils, films, and particles, one must assess the energy density deposited into the specific type of specimen. Since the rate of specimen damage is proportional to the *energy density*, one might expect, to a first approximation, higher damage rates at lower energies (since, assuming that the beam current decreases somewhat linearly with decreasing beam energy, the energy density increases as the beam energy decreases) (after Joy DC, private communication).

C. Tollkamp-Schierjott: Do you think that it is possible to achieve an electron range comparable to the SE escape depth simply by reducing the primary energy of the beam?
Author: The mean free path (λ) for secondary electrons is generally ≈0.5–1 nm in metals and ≈2–5 nm in insulators. It is usual to assume that all emerging secondaries are produced within 5 λ of the surface, which is on the order of 5–25 nm. As discussed by Joy (1985), improved spatial resolution and enhanced contrast can be expected when experiments are carried out under these conditions. Theoretically, for the case of tungsten carbide and gallium arsenide, this range can be obtained by the use of electron beams having energies in the range of ≈0.75–2 keV and 0.25–0.75 keV, respectively.

J. Pawley: While it is true that the total electron current into a flat surface can be made to be zero by judicious choice of incident angle and electron energy, this is seldom true for SEM samples, which tend not to be flat. Consequently, even at low electron energies, charging can and does occur on some areas of most common, nonconducting samples. Have you noticed this sort of problem and, if so, how have you overcome it?
Author: The only one of the four types of samples studied which was "nonconducting" was the chemically modified polydiacetylene. In this sample, some charging was encountered even at 1 keV, and in order to provide acceptable micrographs, a shorter exposure time was used. An alternative technique to decreasing the exposure time in a classical photographic setup is the use of digital image acquisition. For example, a 256 × 256 × 8 bit image, containing little to no observable specimen charging, can be acquired in less than 5 s with the Tracor Northern TN-5600 imaging package. This digital image can be processed and a hard-copy photograph can ultimately be obtained.